Neutron scattering and muon spin relaxation measurements of the noncentrosymmetric antiferromagnet $CeCoGe_3$

M. Smidman,[1,*] D. T. Adroja,[2,†] A. D. Hillier,[2] L. C. Chapon,[3] J. W. Taylor,[2] V. K. Anand,[2] R. P. Singh,[1] M. R. Lees,[1] E. A. Goremychkin,[2,4] M. M. Koza,[3] V. V. Krishnamurthy,[5] D. M. Paul,[1] and G. Balakrishnan[1,‡]

[1]*Department of Physics, University of Warwick, Coventry CV4 7AL, United Kingdom*

[2]*ISIS Facility, STFC, Rutherford Appleton Laboratory, Chilton, Didcot, Oxfordshire OX11 0QX, United Kingdom*

[3]*Institut Laue-Langevin, Boîte Postale 156, 38042 Grenoble Cedex 9, France*

[4]*School of Physics and Astronomy, University of Southampton, Southampton SO17 1BJ, United Kingdom*

[5]*School of Physics, Astronomy and Computational Sciences, George Mason University, Fairfax, Virginia 22030, USA*

(Received 1 August 2013; published 18 October 2013)

The magnetic states of the noncentrosymmetric pressure-induced superconductor $CeCoGe_3$ have been studied with magnetic susceptibility, muon spin relaxation (μSR), single-crystal neutron diffraction, and inelastic neutron scattering (INS). $CeCoGe_3$ exhibits three magnetic phase transitions at $T_{N1} = 21$, $T_{N2} = 12$, and $T_{N3} = 8$ K. The presence of long-range magnetic order below T_{N1} is revealed by the observation of oscillations of the asymmetry in the μSR spectra between 13 and 20 K and a sharp increase in the muon depolarization rate. Single-crystal neutron-diffraction measurements reveal magnetic Bragg peaks consistent with propagation vectors of $\mathbf{k} = (0,0,\frac{2}{3})$ between T_{N1} and T_{N2}, $\mathbf{k} = (0,0,\frac{5}{8})$ between T_{N2} and T_{N3} and $\mathbf{k} = (0,0,\frac{1}{2})$ below T_{N3}. An increase in intensity of the (110) reflection between T_{N1} and T_{N3} also indicates a ferromagnetic component in these phases. These measurements are consistent with an equal moment two-up two-down magnetic structure below T_{N3} with a magnetic moment of $0.405(5)\mu_B$/Ce. Above T_{N2}, the results are consistent with an equal moment two-up one-down structure with a moment of $0.360(6)\mu_B$/Ce. INS studies reveal two crystal-electric-field (CEF) excitations at $\sim$19 and $\sim$27 meV. From an analysis with a CEF model, the wave functions of the $J = \frac{5}{2}$ multiplet are evaluated along with a prediction for the magnitude and direction of the ground-state magnetic moment. Our model correctly predicts that the moments order along the c axis, but the observed magnetic moment of $0.405(5)\mu_B$ is reduced compared to the predicted moment of $1.0\mu_B$. This is ascribed to hybridization between the localized Ce^{3+} f electrons and the conduction band. This suggests that $CeCoGe_3$ has a degree of hybridization between that of $CeRhGe_3$ and the noncentrosymmetric superconductor $CeRhSi_3$.

DOI: 10.1103/PhysRevB.88.134416 PACS number(s): 75.30.Mb, 75.10.Dg, 75.20.Hr, 75.30.Gw

I. INTRODUCTION

The coexistence of superconductivity (SC) and magnetism in heavy fermion (HF) compounds has attracted considerable research interest recently. In particular, several HF systems appear to exhibit unconventional SC close to a quantum critical point (QCP). On tuning the electronic ground state (GS) of these systems by doping, pressure or the application of magnetic fields, the SC appears in regions where the magnetic order is being suppressed.[1,2] There is great interest, therefore, in understanding this phenomenon and, in particular, the role of magnetic fluctuations in potentially mediating the SC of these compounds. Most of the compounds which display HF SC have centrosymmetric crystal structures in which the Cooper pairs condense in either spin-singlet or spin-triplet states. However, several cerium-based compounds with noncentrosymmetric structures have recently been reported to exhibit SC. The first HF noncentrosymmetric superconductor (NCS) reported was $CePt_3Si$ where antiferromagnetic (AFM) order ($T_N = 2.2$ K) and SC ($T_c = 0.75$ K) coexist at ambient pressure.[3] In NCSs, a finite antisymmetric spin-orbit coupling (ASOC) lifts the spin degeneracy of the conduction bands, allowing for the mixture of spin-singlet and spin-triplet pairing states.[4]

We report results of neutron scattering and muon spin relaxation (μSR) measurements of the NCS $CeCoGe_3$. This is a member of the $CeTX_3$ (T = transition metal, X = Si or Ge) series of compounds which crystallize in the noncentrosymmetric tetragonal $BaNiSn_3$-type structure (space group $I4mm$). In particular, the lack of a mirror plane perpendicular to [001] leads to a Rashba-type ASOC.[5] $CeCoGe_3$ orders antiferromagnetically at ambient pressure with three magnetic phases ($T_{N1} = 21$, $T_{N2} = 12$, and $T_{N3} = 8$ K).[6,7] T_{N1} decreases as a function of applied pressure, and there is an onset of SC for $p > 4.3$ GPa with a T_c of 0.7 K at 5.5 GPa.[8] SC is also observed in $CeRhSi_3$ ($p > 1.2$ GPa),[9] $CeIrSi_3$ ($p > 1.8$ GPa) (Ref. 10), and $CeIrGe_3$ ($p > 20$ GPa).[11] The superconducting states of these compounds display highly unconventional properties. As well as regions of coexistence with AFM order, the upper critical field is highly anisotropic, vastly exceeding the Pauli limiting field along the c axis.[12] However, some members of the $CeTX_3$ family, such as $CeCoSi_3$ and $CeRuSi_3$, do not order magnetically and are intermediate-valence compounds.[13,14]

The range of observed magnetic properties in the $CeTX_3$ series has previously been discussed in the context of the Doniach phase diagram[5,15–17] with competition between the intersite Ruderman-Kittel-Kasuya-Yosida interaction which favors magnetic ordering and the on-site Kondo effect which leads to a nonmagnetic singlet ground state. However, further studies are necessary to characterize the magnetic states of the $CeTX_3$ series. Knowledge of the magnetic ground states and crystal-electric-field (CEF) levels will aid in understanding

the relationship between SC and magnetism in the CeTX_3 compounds and allows detailed comparisons between members of the series. In particular, the role of hybridization in determining the phase diagram can be examined. $CeCoGe_3$ can be considered a strongly correlated system with an electronic specific heat coefficient of $\gamma = 32$ mJ mol^{-1} K^{-2} and an enhanced cyclotron mass of $10m_e$, where m_e is the free-electron mass.[7,18] The proximity of the compound to quantum criticality has been studied in the $CeCoGe_{3-x}Si_x$ system where the substitution of Si increases the chemical pressure. Interestingly, although antiferromagnetism is suppressed for $x = 1.2$ and a quantum critical region with non-Fermi-liquid behavior is observed for $1 < x < 1.5$, no SC was reported down to 0.5 K.[13,19] This is in contrast to the superconducting behavior observed for the $x = 0$ compound with applied hydrostatic pressure.

As well as being an unconventional superconductor,[12] $CeCoGe_3$ has the highest magnetic ordering temperature ($T_{N1} = 21$ K) of any of the CeTX_3 compounds and exhibits a complex temperature-pressure phase diagram.[20,21] Specific heat measurements of single crystals reveal that, under a pressure of $p = 0.8$ GPa, a fourth transition is observed at 15.3 K in addition to those observed under ambient conditions.[20] The temperature of this transition does not shift with pressure, whereas, T_{N1} is suppressed until it meets the pressure-induced phase at $p = 1.5$ GPa. In turn, the transition temperature of this phase is suppressed upon further increasing pressure until it merges with T_{N2}. The $T - P$ phase diagram shows a series of steplike decreases in the magnetic ordering temperature. A total of six phases in the phase diagram were suggested from single-crystal measurements up to 7 GPa, whereas, eight were observed in polycrystalline samples up to 2 GPa.[20] The magnetic order is suppressed at $p = 5.5$ GPa, and there is a region of coexistence with SC. The lack of steplike transitions above 3.1 GPa could indicate a change in magnetic structure which may be important for understanding the emergence of SC in the system.

The magnetic structure of $CeCoGe_3$ has previously been studied at ambient pressure using single-crystal neutron diffraction in a zero field where two propagation vectors were observed at 2.9 K, $\mathbf{k}_1 = (0,0,\frac{1}{2})$ and $\mathbf{k}_2 = (0,0,\frac{3}{4})$.[22] Powder-neutron-diffraction measurements also indicate the presence of $\mathbf{k}_1$ at 2 K.[23] In this study, we have determined the magnetic propagation vector in a zero field for each of the three magnetic phases using single-crystal neutron diffraction. We are then able to propose magnetic structures for the phases above T_{N2} and below T_{N3}. We report the temperature dependence of magnetic Bragg reflections from 2 to 35 K. The presence of long-range magnetic order is also revealed by μSR measurements where oscillations are observed in the spectra below T_{N1}. Single-crystal susceptibility and magnetization measurements were previously used to suggest a CEF scheme with a ground-state doublet consisting of the $|\pm\frac{1}{2}\rangle$ states.[7] We use inelastic neutron scattering (INS) to directly measure transitions from the ground state to the excited CEF levels and are able to find an energy-level scheme and a set of wave functions compatible with both INS and magnetic-susceptibility measurements. We are also able to compare the degree of hybridization in $CeCoGe_3$ with other compounds in the series.

II. EXPERIMENTAL DETAILS

Polycrystalline samples of $CeCoGe_3$ and $LaCoGe_3$ were prepared by arc melting the constituent elements (Ce: 99.99%, La: 99.99%, Co: 99.95%, and Ge: 99.999%) in an argon atmosphere on a water-cooled copper hearth. After being flipped and remelted several times, the boules were wrapped in tantalum foil and were annealed at 900 °C for a week under a dynamic vacuum at better than 10^{-6} Torr. Powder-x-ray-diffraction measurements were carried out using a Panalytical X-Pert Pro diffractometer. Single crystals were grown by melting polycrystalline material with a bismuth flux following the previously reported technique.[7] Platelike single crystals were obtained with faces perpendicular to [001] and were checked using an x-ray Laue imaging system. Excess bismuth was removed by washing the crystals with a solution of 1:1 nitric acid. That the crystals had the correct stoichiometry was confirmed by scanning electron microscopy measurements. Magnetic-susceptibility measurements were performed using a Quantum Design Magnetic Property Measurement System superconducting quantum interference device magnetometer.

Inelastic neutron scattering and μSR measurements were performed in the ISIS facility at the Rutherford Appleton Laboratory, U.K. INS measurements were carried out on the MARI and MERLIN spectrometers. The samples were wrapped in thin Al foil and were mounted inside a thin-walled cylindrical Al can, which was cooled down to 4.5 K inside a closed cycle refrigerator with He-exchange gas around the samples. Incident energies of 10 and 40 meV were used on MARI, whereas, 15-meV energies were used on MERLIN, selected via a Fermi chopper. Further low-energy INS measurements were carried out on the IN6 spectrometer at the Institut Laue-Langevin, France, with an incident energy of 3.1 meV. μSR measurements were carried out on the μSR spectrometer with the detectors in the longitudinal configuration. Spin-polarized muon pulses were implanted into the sample, and positrons from the resulting decay were collected in positions either forward or backward of the initial muon spin direction. The asymmetry is calculated by

$$G_z(t) = \frac{N_F - \alpha N_B}{N_F + \alpha N_B}, \quad (1)$$

where N_F and N_B are the number of counts at the detectors in the forward and backward positions and α is a constant determined from calibration measurements made in the paramagnetic state with a small applied transverse magnetic field. The maximum asymmetry for an ideal pair of detectors is $\frac{1}{3}$, but this is lower for a real spectrometer.[24] The sample was mounted on a silver plate using GE varnish and was cooled in a standard cryostat down to 1.5 K with He-exchange gas around the sample.

Single-crystal neutron-diffraction measurements were carried out on the D10 instrument at the Institut Laue-Langevin, France. The sample was mounted on an aluminum pin and was cooled in a helium-flow cryostat operating down to 2 K. The instrument was operated in the four-circle configuration. An incident wavelength of 2.36 Å was selected using a pyrolytic graphite monochromator. A vertically focused pyrolytic graphite analyzer was used to reduce the background signal.

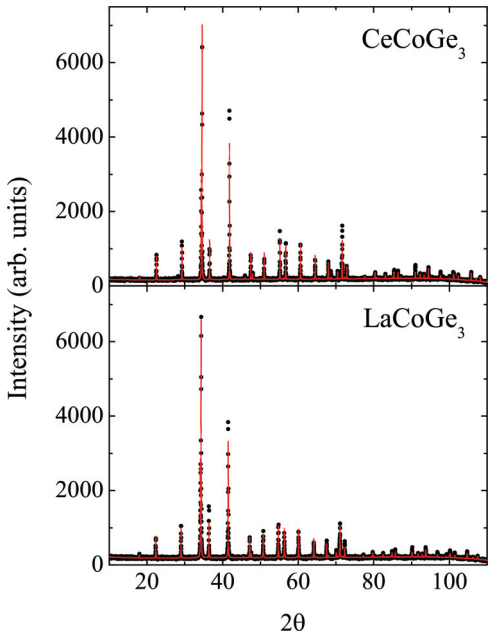

FIG. 1. (Color online) Powder x-ray diffraction measurements of polycrystalline $CeCoGe_3$ and $LaCoGe_3$. The solid lines show the Rietveld refinements, the results of which are given in Table I.

After passing through the analyzer, neutrons were detected using a single ^{3}He detector.

III. RESULTS AND DISCUSSION

A. Powder-x-ray diffraction

Powder x-ray diffraction measurements were carried out on polycrystalline samples of $CeCoGe_3$ and the isostructural nonmagnetic $LaCoGe_3$ at 300 K. A Rietveld refinement was carried out on both samples using the TOPAS software.[25] The data and refinement are shown in Fig. 1. One small impurity peak was detectable in $CeCoGe_3$ (∼1% of the intensity of the maximum sample peak), whereas, none were observed in $LaCoGe_3$, indicating that the samples are very nearly single phase. The site occupancies were all fixed at 100%. The results of the refinements are displayed in Table I. The values of the lattice parameters are in agreement with previously reported values.[6,23]

TABLE I. Results of the refinements of powder-x-ray-diffraction measurements on $CeCoGe_3$ and $LaCoGe_3$. The lattice parameters, weighted profile factor (R_{wp}), and the atomic positions are displayed.

	$CeCoGe_3$	$LaCoGe_3$	
a (Å)	4.32042(4)	4.35083(7)	
c (Å)	9.83484(11)	9.87155(2)	
R_{wp}	10.33	8.86	
	x	y	z
Ce	0	0	0
Co	0	0	0.666(7)
Ge1	0	0	0.4281(6)
Ge2	0	0.5	0.7578(5)
La	0	0	0
Co	0	0	0.6628(7)
Ge1	0	0	0.4285(6)
Ge2	0	0.5	0.7556(5)

B. Muon spin relaxation

To investigate the nature of magnetic ordering in $CeCoGe_3$, we measured the zero-field muon spin relaxation of a polycrystalline sample. In the range of 13 K $< T <$ 20 K, oscillations of the asymmetry are observed in the μSR spectra, indicating the presence of long-range magnetic order (Figs. 2 and 3). The presence of an oscillation at 20 K (Fig. 3) as well as a reduced initial asymmetry indicates that the system is ordered at 20 K. However, at 21 K, no oscillations are observed, and the initial asymmetry reaches the full value for the instrument, indicating that T_{N1} lies between 20 and 21 K. The spectra were fitted with

$$G_z(t) = \sum_{i=1}^{n} A_i \cos(\gamma_\mu B_i t + \phi) e^{-(\sigma_i t)^2/2} + A_0 e^{-\lambda t} + A_{bg}, \quad (2)$$

where A_i's are the amplitudes of the oscillatory component, A_0 is the initial amplitude of the exponential decay, B_i's are the magnetic fields at the muon site i, σ_i is the Gaussian decay

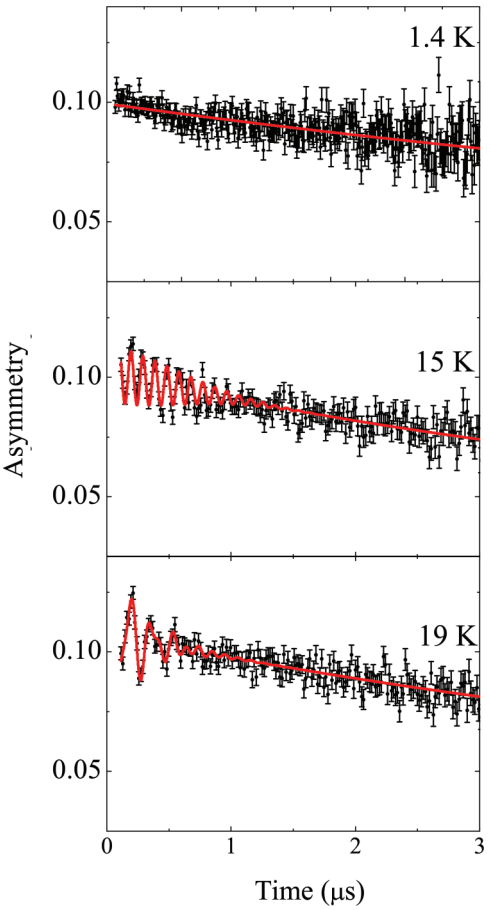

FIG. 2. (Color online) μSR spectra measured at three temperatures. At 19 K, two frequencies could be observed, whereas, at 15 K, only one frequency was observed. At 1.4 K, no oscillations in the spectra were observed. The solid lines show the fits as described in the text.

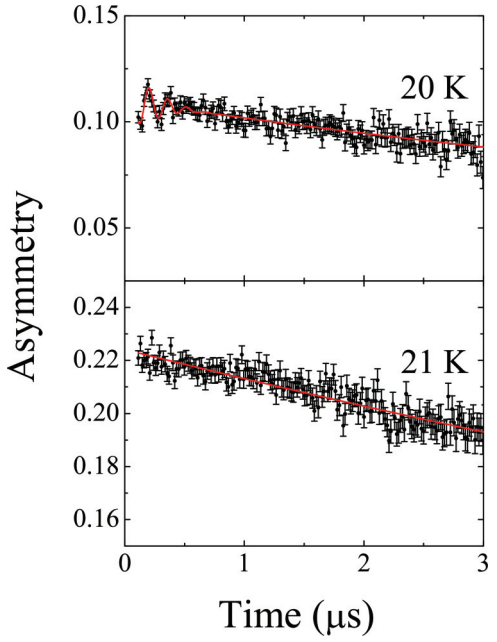

FIG. 3. (Color online) μSR spectra measured at 20 and 21 K. At 20 K, one frequency is observed in the spectrum, and the initial asymmetry is reduced, whereas, at 21 K, no oscillations are observed, and the initial asymmetry reaches the full value for the instrument. The solid lines show the fits as described in the text.

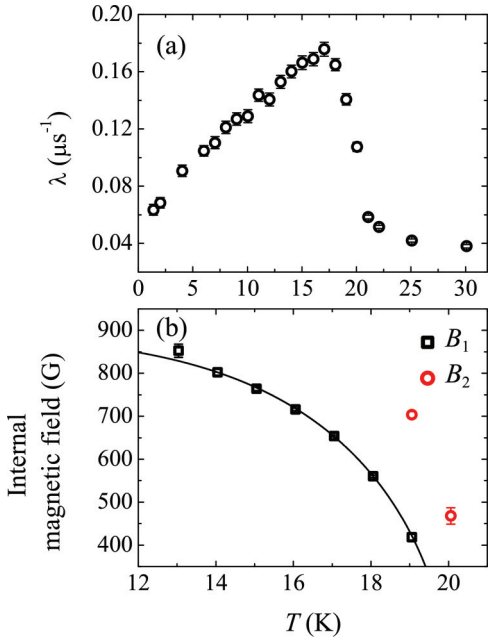

FIG. 4. (Color online) (a) The muon depolarization rate as a function of temperature. (b) The internal fields deduced from the frequencies of the oscillations observed in zero-field μSR spectra. The solid curve is a fit of B_1 to a mean-field model described in the text.

rate, λ is the muon depolarization rate, ϕ is the common phase, $\gamma_\mu/2\pi = 135.53$ MHz T^{-1}, and A_{bg} is the background. All the oscillatory spectra could be fitted with one internal magnetic field ($n = 1$) apart from at 19 K when it was fitted with two internal magnetic fields ($n = 2$). This implies that there are at least two muon sites, but below 19 K, it is likely that B_2 exceeds the maximum internal field detectable on the μSR spectrometer due to the pulse width of the ISIS muon beam. Below 13 K, the spectra were fitted with just an exponential decay term. The temperature dependence of one of the internal fields was fitted with

$$B(T) = B(0)\left[1 - \left(\frac{T}{T_N}\right)^{\alpha}\right]^{\beta}. \quad (3)$$

With β fixed at 0.5 for a mean-field magnet, values of $B(0) = 889(16)$ G, $\alpha = 4.7(4)$, and $T_N = 20.12(8)$ K were obtained (Fig. 4). A good fit with $\beta = 0.5$ means the observations are consistent with that of a mean-field magnet. The large value of α indicates complex interactions between the magnetic moments. It was also possible to fit the data with $\beta = 0.367$ and 0.326 for a three-dimensional Heisenberg and Ising model, respectively.[26] However, fits with both these values of β gave values of $T_N < 20$ K, and poor fits were obtained for $T_N > 20$ K. Since the presence of long-range magnetic order has been observed at 20 K (Fig. 3), the data are incompatible with these models. The muon depolarization rate (λ) was found to suddenly increase at T_{N1}, indicating a transition between the paramagnetic and the ordered states. However, λ does not show a significant anomaly at either T_{N2} or T_{N3} where there is a rearrangement of the spins and a change in the magnetic structure. The initial value of the asymmetry (A_z) as a function of applied longitudinal field at 1.4 K is shown in Fig. 5. This is the longitudinal component and has been normalized such that $A_z = 1$ corresponds to the muon being fully decoupled from its local environment. A fit has been made using the expression described in Ref. 27. An internal field of 1080(40) G was obtained, which is in approximate agreement with that deduced from the zero-field data, despite a change in magnetic structure between 13 and 1.4 K.

C. Single-crystal neutron diffraction

Single-crystal neutron-diffraction measurements were carried out in each of the three magnetically ordered phases on the D10 diffractometer. Figure 6 shows elastic scans made across (10l) at different temperatures. This reveals that,

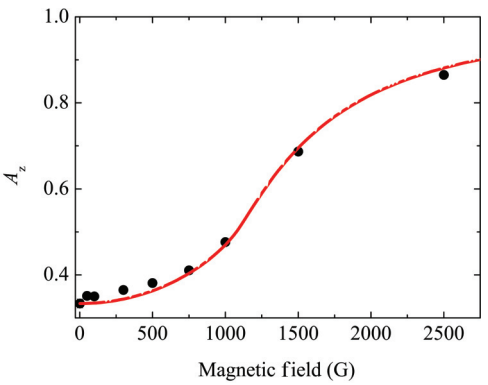

FIG. 5. (Color online) The normalized longitudinal component of the initial asymmetry (A_z) as a function of an applied magnetic field at 1.4 K. The solid line shows a fit described in the text.

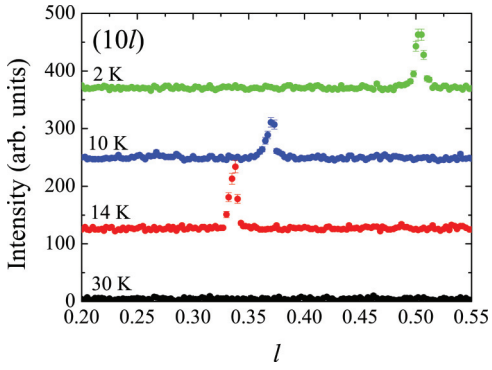

FIG. 6. (Color online) Elastic scans made across (10l) at four temperatures. No peak is observed above T_{N1}. Below 2 K, a peak is observed at $l = \frac{1}{2}$, which shifts to $l = \frac{3}{8}$ at 10 K and $l = \frac{1}{3}$ at 14 K.

below 20 K, additional peaks for noninteger l are observed, indicating the onset of antiferromagnetic ordering. At 2 K, the additional peak is at $l = \frac{1}{2}$, at 10 K, it is at $l = \frac{3}{8}$, and at 14 K, it is at $l = \frac{1}{3}$. Since the (100) peak is forbidden for a body-centered structure, this indicates a propagation vector of $\mathbf{k} = (0,0,\frac{1}{2})$ below T_{N3}, $\mathbf{k} = (0,0,\frac{5}{8})$ for $T_{N3} < T < T_{N2}$, and $\mathbf{k} = (0,0,\frac{2}{3})$ for $T_{N2} < T < T_{N1}$. Figure 7 shows the intensity of the (110) reflection between 2 and 25 K. The increase in integrated intensity of this nuclear peak for $T_{N3} < T < T_{N1}$ indicates the presence of an additional ferromagnetic (FM) component for these two magnetic phases. The propagation vector of $\mathbf{k} = (0,0,\frac{1}{2})$ agrees with the previous single-crystal neutron-diffraction measurements.[22] However, as shown in Fig. 6, we do not see a peak at $(1\,0\,\frac{1}{4})$ as previously observed, nor do we observe any evidence for a two component magnetic structure. However at 8 K, just above T_{N3}, coexistence of the $(1\,0\,\frac{1}{2})$ and $(1\,0\,\frac{3}{8})$ reflections are observed (Fig. 8), indicating a first-order transition between the phases. This is also supported by the observation of hysteresis in magnetic isotherms at 3 K.[6]

At 35 K, in the paramagnetic state, the intensities were collected for all the allowed experimentally accessible reflections (hkl). In each magnetic phase, intensities were collected for the reflections $(hkl) \pm \mathbf{k}$. The intensities of 104 magnetic reflections were collected at 2 and 14 K, whereas,

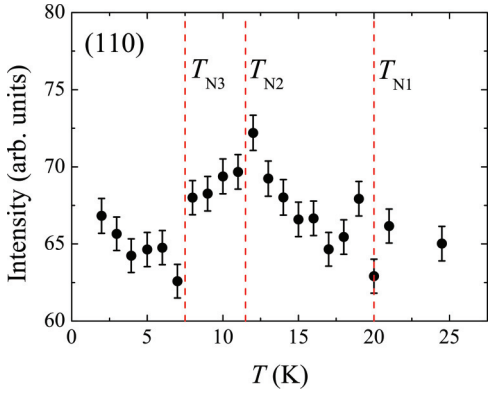

FIG. 7. (Color online) The temperature dependence integrated intensity of the (110) reflection. An increase in the intensity between T_{N3} and T_{N1} indicates there is a ferromagnetic contribution in these phases.

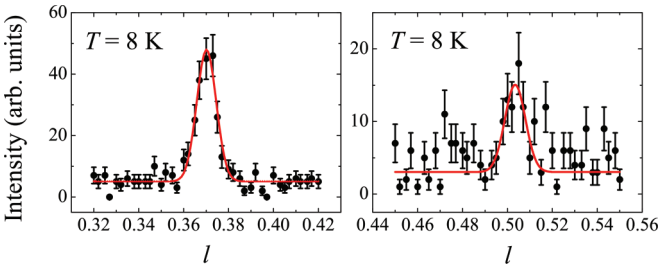

FIG. 8. (Color online) Elastic scans made across (10l) at 8 K. At this temperature, there is a coexistence between the peaks at $l = \frac{3}{8}$ and $l = \frac{1}{2}$.

57 were collected at 10 K. No magnetic peaks were observed corresponding to (00l), indicating that, in all three phases, the magnetic moments point along the c axis. A symmetry analysis of each phase using SARAh (Ref. 28) shows that Γ_2 is the only irreducible representation of the little group (G_k) with the moments along the c axis. Both the crystal and the magnetic structures of each phase were fitted using FULLPROF.[29] With the scale factor and extinction parameters fixed from the results of the crystal structure refinement, the only free parameter in the refinements of the magnetic phases was the magnetic moment on the Ce atoms. An R factor of 10.9 was obtained for the refinement of the crystal structure, 21.5 for the magnetic phase at 2 K, 24.3 at 10 K, and 22 at 14 K. Plots of F_{calc} vs F_{obs} for all the refinements are shown in Fig. 9. The introduction of a global phase ϕ to a magnetic structure leaves the neutron-diffraction pattern unchanged. However, for the phase at 2 K with $\mathbf{k} = (0,0,\frac{1}{2})$, selecting $\phi = \pi/4$ gives an equal moment on each Ce site of $0.405(5)\mu_B$. This structure has a two-up two-down configuration along the c axis [Fig. 10(c)]. Similarly, for the phase at 14 K with $\mathbf{k} = (0,0,\frac{2}{3})$, selecting $\phi = 0$ gives a modulated structure along the c axis with an up moment of $0.485(6)\mu_B$ followed by two down moments of $0.243(3)\mu_B$. The addition of a FM component

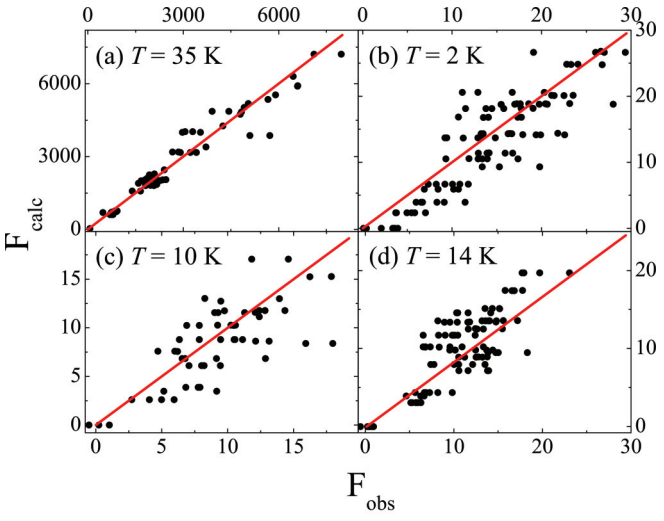

FIG. 9. (Color online) Plots of the calculated vs observed values of F_{hkl} for the refinement of (a) the crystal structure at 35 K and (b)–(d) the magnetic structure in the three magnetic phases. The solid lines indicate where $F_{calc} = F_{obs}$.

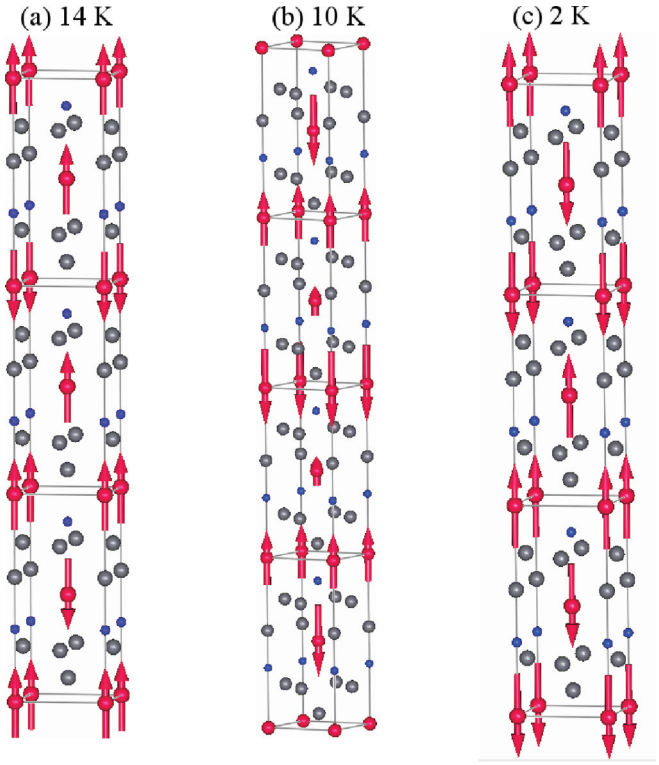

FIG. 10. (Color online) The crystal structure of $CeCoGe_3$ where the Ce atoms are in red, the Co atoms are in blue, and the Ge atoms are in gray. The arrows depict the magnetic moments on the Ce atoms. (a) The proposed magnetic structure at 14 K consists of the antiferromagnetic component with a global phase $\phi = 0$ and a ferromagnetic component to give an equal moment two-up one-down structure. (b) The antiferromagnet component ($\phi = 0$) at 10 K for one half of the magnetic unit cell. (c) The magnetic structure at 2 K with $\phi = \pi/4$ to give an equal moment two-up two-down structure.

of $-0.125\mu_B$/Ce gives a constant moment two-up one-down configuration as shown in Fig. 10(a). A FM component is observed in this phase (Fig. 7), and this equal moment solution is compatible with magnetization results.[7] For the phase at 10 K with $\mathbf{k} = (0,0,\frac{5}{8})$, we were unable to deduce a global phase ϕ to which a FM component could be added to give an equal moment solution. A simple three-up one-down structure as previously suggested for this phase from magnetization measurements[7] is not compatible with this propagation vector. The antiferromagnetic component with $\phi = 0$ is shown in Fig. 10(b) for half of the magnetic unit cell. However, as shown in Fig. 7, there is also a ferromagnetic component in this phase, and further measurements of the nuclear reflections at 10 K would be required to determine the size of this contribution.

D. Inelastic neutron scattering

To obtain information about the CEF scheme and the magnetic excitations of the ordered state, INS measurements were carried out on polycrystalline samples of $CeCoGe_3$ and $LaCoGe_3$ using the MARI spectrometer with incident neutron energies (E_i) of 10 and 40 meV. $LaCoGe_3$ is nonmagnetic and isostructural to $CeCoGe_3$, and the measurements were used to estimate the phonon contribution to the scattering. Color-coded plots of the INS intensity of $CeCoGe_3$ are

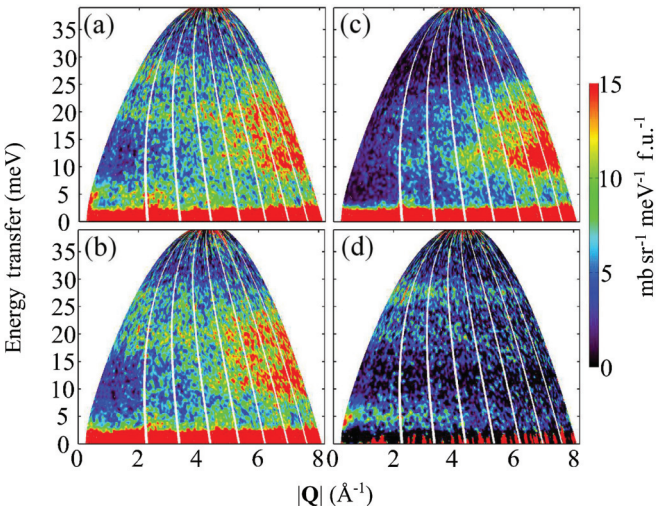

FIG. 11. (Color online) Color-coded plots of the inelastic neutron scattering intensity with an incident energy of 40 meV [in units of mb sr^{-1} meV^{-1} f.u.$^{-1}$ (where f.u. represents formula units)] for (a) $CeCoGe_3$ at 4 K, (b) $CeCoGe_3$ at 25 K, and (c) $LaCoGe_3$ at 5 K. The magnetic scattering of $CeCoGe_3$ at 4 K, obtained by subtracting the phonon contribution of $CeCoGe_3$ (see text), is shown in (d).

shown in Figs. 11(a) and 11(b) at 4 and 25 K, respectively, whereas, the scattering of $LaCoGe_3$ is shown Fig. 11(c). In both the magnetically ordered and the paramagnetic states, two inelastic excitations are observed with a significant intensity at low scattering vectors ($\mathbf{Q}$). These are absent in the scattering of nonmagnetic $LaCoGe_3$, indicating they are magnetic in origin. The excitations have a maximum intensity at approximately 19 and 27 meV. These can be seen in Fig. 11(d), which shows the magnetic scattering [$S_{mag}(Q,\omega)$] obtained from $S_{Ce}(Q,\omega)$-$\alpha S_{La}(Q,\omega)$, where $\alpha = 0.9$, the ratio of the scattering cross sections of $CeCoGe_3$ and $LaCoGe_3$. The scattering intensity decreases with $|\mathbf{Q}|$ as expected for CEF excitations. The presence of two CEF excitations is expected for a Ce^{3+} ion in a tetragonal CEF since, according to Kramers theorem, provided time-reversal symmetry is preserved, the energy levels of a system with an odd number of electrons must remain doubly degenerate. Therefore, the sixfold $J = \frac{5}{2}$ ground state can be split into a maximum of three doublets in the paramagnetic state.

Also revealed in the 4-K data is an additional excitation with a maximum at around 4.5 meV. This excitation is not present at 25 K [Fig. 11(b)] where, instead, the elastic line is broader. This indicates the presence of spin waves in the ordered state at 4 K with an energy scale of approximately 4.5 meV for the zone-boundary magnons. Interestingly, the spin-wave peak in $CeRhGe_3$ is observed at around 3 meV, and the compound orders at $T_{N1} = 14.5$ K.[30] Therefore, the spin-wave energy appears to similarly scale with T_{N1} in both $CeRhGe_3$ and $CeCoGe_3$. Additional low-energy measurements on IN6 with an incident energy of 3.1 meV display a lack of magnetic scattering below 2 meV at 4 K, indicating a spin gap in the magnon spectrum. In the paramagnetic state, the spectral weight is shifted towards the elastic line, and quasielastic scattering (QES) is observed. This is additional magnetic scattering, centered on the elastic line but with a linewidth

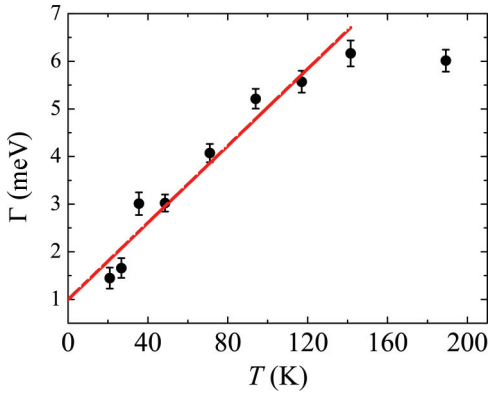

FIG. 12. (Color online) The temperature dependence of the quasielastic linewidth (HWHM) obtained from fitting data measured with an incident energy of 15 meV (see text). A linear fit of the data between 20 and 150 K is displayed.

broader than the instrument resolution. Further measurements were performed in the paramagnetic state between 20 and 200 K on the MERLIN spectrometer with an incident energy of 15 meV. The temperature dependence of the half width at half maximum (HWHM) (Γ) is shown in Fig. 12. The data were fitted with an elastic line resolution function and an additional Lorentzian function to model the quasielastic component. The widths of the elastic component were fixed from measurements of vanadium with the same incident energy and frequency of the Fermi chopper. An estimate of the Kondo temperature (T_K) can be obtained from the value of Γ at 0 K. From a linear fit to the data, we estimate $T_K = 11(3)$ K. This is on the same order as the ordering temperature $T_{N1} = 21$ K. A linear dependence of the QES linewidth with temperature is expected until the thermal energy approaches the splitting of the first excited CEF level.[31] The first CEF excitation is at 19 meV (~220 K), which may explain the deviation from linear behavior observed at 190 K. It was also possible to fit the data to a $T^{1/2}$ dependence. This behavior has been observed in the linewidth of the QES scattering in other HF systems.[32] However, this fit yields a negative value of $\Gamma(0)$ for which we have no physical interpretation and, therefore, has not been displayed.

Cuts of $S_{mag}(Q,\omega)$ were made by integrating across low values of $|\mathbf{Q}|$ (0–3 Å^{-1}). These are shown for $E_i = 40$ meV in Fig. 13 and for $E_i = 10$ meV in Fig. 14. The data were analyzed with the following Hamiltonian for a Ce^{3+} ion at a site with tetragonal point symmetry:

$$\mathcal{H}_{CF} = B_2^0 O_2^0 + B_4^0 O_4^0 + B_4^4 O_4^4, \quad (4)$$

where B_n^m are CEF parameters and O_n^m are the Stevens operator equivalents. Using the fact that Stevens operator equivalents can be expressed in terms of angular momentum operators, the CEF wave functions and energies may be determined from diagonalizing $\mathcal{H}_{CF}$.[33,34] We sought to find a CEF scheme compatible with both INS and magnetic susceptibility data. B_2^0 can be estimated for isotropic exchange interactions from the high-temperature magnetic susceptibility[35] using the relation,

$$B_2^0 = \frac{10k_B(\theta_{ab} - \theta_c)}{3(2J-1)(2J+3)}, \quad (5)$$

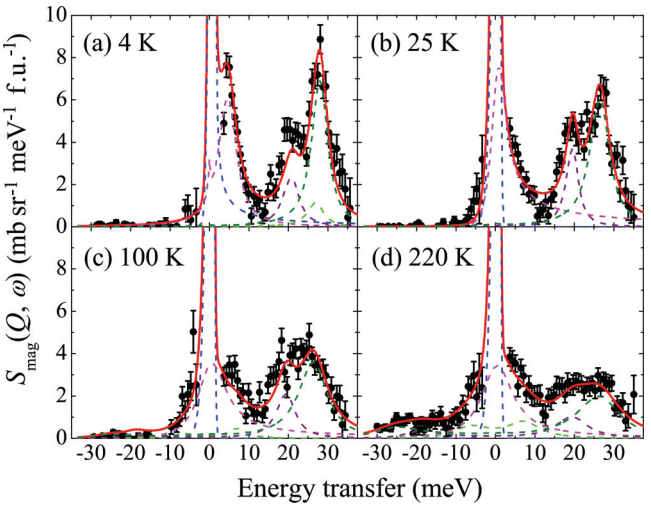

FIG. 13. (Color online) Cuts of $S_{mag}(Q,\omega)$ with an incident energy of 40 meV integrated over $|\mathbf{Q}|$ from 0 to 3 Å^{-1}. The solid lines show fits made to a CEF model described in the text. The components of the fits are shown with dashed lines.

where θ_{ab} and θ_c are the Curie-Weiss temperatures for fields applied in the ab plane and along the c axis, respectively. Using the previously obtained values,[7] B_2^0 is calculated to be -0.376 meV. In particular, since $\theta_{ab} < \theta_c$, a negative B_2^0 is anticipated. We then fitted the INS data in the paramagnetic state with $E_i = 10$ and 40 meV to obtain values of B_n^m. Initially, we fixed $B_2^0 = -0.376$ meV and varied B_4^0 and B_4^4. In the final fit, all three CEF parameters were varied. The fits are shown in Figs. 13(b)–13(d) and 14(b), and it can be seen that there is a good fit to the INS data. Using these values of B_n^m, a fit

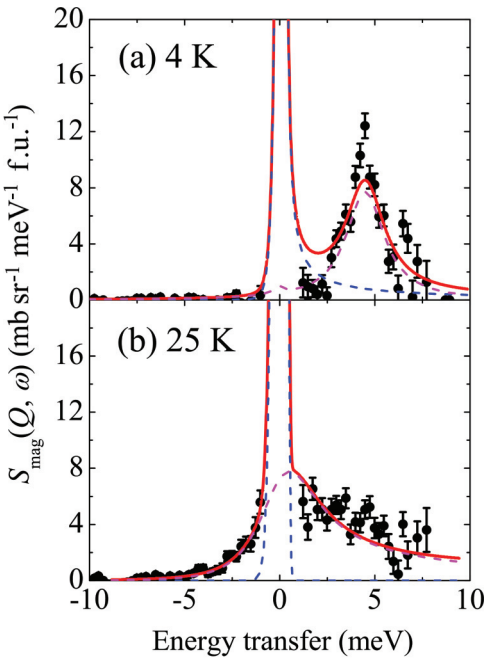

FIG. 14. (Color online) Cuts of $S_{mag}(Q,\omega)$ with an incident energy of 10 meV integrated over $|\mathbf{Q}|$ from 0 to 2 Å^{-1}. Fits are made to a CEF model (see text). The components of the fits are shown with dashed lines.

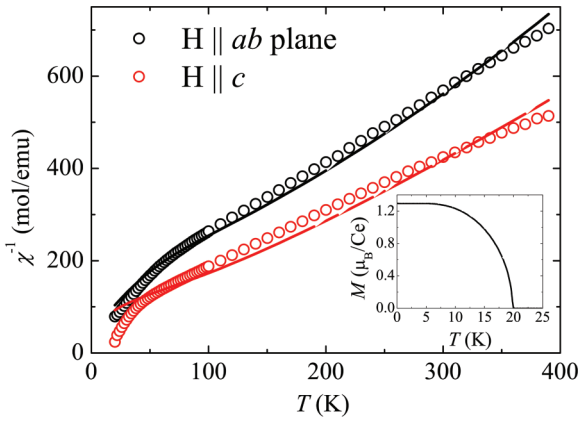

FIG. 15. (Color online) The single-crystal susceptibility between 20 and 390 K with an applied field of 1000 G. The solid lines show fits to a CEF model (see text). The CEF parameters were fixed from the INS data, but anisotropic molecular fields (λ_{ab} and λ_c) and temperature-independent susceptibilities were fitted. The inset shows a self-consistent mean-field calculation of the magnetization per cerium atom using the fitted CEF parameters and a molecular-field parameter of 38.9 mol/emu.

was made to the single-crystal susceptibility data, which show reasonably good agreement (Fig. 15). Simultaneously fitting the magnetic susceptibility and the INS data at 25 K led to similar values of B_n^m. At 4 K, in the ordered state, an additional peak is observed in $S_{\rm mag}(Q,\omega)$ at around 4.5 meV. Although the full treatment of these data would require a calculation of the spin-wave excitations, we sought to determine if the addition of an internal magnetic field could satisfactorily account for this peak in the ordered state. Since the magnetic moments lie along the c axis below $T_{\rm N1}$, we fitted $S_{\rm mag}(Q,\omega)$ with a finite internal field B_z, allowing B_4^0 and B_4^4 to vary. A small change in the CEF parameters was allowed below $T_{\rm N}$. This is expected due to small changes in the lattice parameters upon magnetic ordering. As shown in Figs. 13(a) and 14(a), a B_z of 1.69(9) meV gives a good fit to the data. The resulting CEF parameters are shown in Table II. The wave functions calculated for the paramagnetic state are

$$\begin{aligned} |\psi_1^{\pm}\rangle &= 0.8185\left|\pm\tfrac{5}{2}\right\rangle - 0.5745\left|\mp\tfrac{3}{2}\right\rangle, \\ |\psi_2^{\pm}\rangle &= \left|\pm\tfrac{1}{2}\right\rangle, \\ |\psi_3^{\pm}\rangle &= 0.8185\left|\pm\tfrac{3}{2}\right\rangle + 0.5745\left|\mp\tfrac{5}{2}\right\rangle \end{aligned} \tag{6}$$

$\psi_1(\Gamma_6(1))$ is predicted to be the GS wave function, whereas, $\psi_2(\Gamma_7)$ is 19.3 meV and $\psi_3(\Gamma_6(2))$ is 26.4 meV above the GS. The GS magnetic moments of the cerium atoms in the ab plane ($\langle\mu_x\rangle$) and along the c axis ($\langle\mu_z\rangle$) can be calculated from

$$\begin{aligned} \langle\mu_z\rangle &= \langle\psi_1^{\pm}|g_J J_z|\psi_1^{\pm}\rangle, \\ \langle\mu_x\rangle &= \langle\psi_1^{\mp}|\frac{g_J}{2}(J^+ + J^-)|\psi_1^{\pm}\rangle. \end{aligned} \tag{7}$$

The magnitude of $\langle\mu_z\rangle$ is calculated to be $1.01\mu_{\rm B}$, whereas, the magnitude of $\langle\mu_x\rangle$ is calculated to be $0.9\mu_{\rm B}$. A self-consistent mean-field calculation of the magnetization shown in the inset of Fig. 15 gives a ground-state magnetic moment of $1.3\mu_{\rm B}$. A molecular-field parameter of $\lambda = 38.9$ mol/emu was chosen to correctly reproduce the observed value of

TABLE II. The parameters obtained from fitting $S_{\rm mag}(Q,\omega)$ from INS and magnetic-susceptibility data. B_m^n's were obtained from fitting the INS data. At 4 K, the value of B_2^0 was fixed, whereas, the other two CEF parameters were allowed to vary. The Lorentzian linewidths of the quasielastic scattering ($\Gamma_{\rm QES}$) and the first and second CEF excitations (Γ_{ψ_2} and Γ_{ψ_3}) are also displayed. The remaining parameters are obtained from fitting the magnetic susceptibility with anisotropic molecular-field parameters (λ_{ab} and λ_0^c) as well as temperature-independent susceptibilities (χ_0^{ab} and χ_0^c).

	4 K	25 K
B_2^0 (meV)	−0.61	−0.61(4)
B_4^0 (meV)	−0.013(3)	−0.007(2)
B_4^4 (meV)	0.412(8)	0.463(8)
$\Gamma_{\rm QES}$ (meV)		1.9(3)
Γ_{ψ_2} (meV)	2.5(2)	1.6(3)
Γ_{ψ_3} (meV)	2.3(2)	2.9(3)
λ_{ab} (mol/emu)		−40.9
λ_c (mol/emu)		−52.0
χ_0^{ab} ($\times10^{-3}$ emu/mol)		−0.404
χ_0^c ($\times10^{-3}$ emu/mol)		−1.936

$T_{\rm N1}$, and this is in good agreement with the values shown in Table II. However, the refinement of the single-crystal neutron-diffraction data at 2 K predicts a moment along the c axis of $0.405(5)\mu_{\rm B}$. This implies there is a reduction in the cerium moment due to hybridization between the GS and the conduction electrons. By considering the magnetocrystalline anisotropy energy (E_a), the moment is predicted to lie along the c axis for a negative B_2^0 and the ψ_1 GS.[36] Therefore, our CEF model correctly predicts the direction of the observed magnetic moment. From previous studies of the magnetic susceptibility, a CEF scheme with a GS of $|\pm\frac{1}{2}\rangle$ was suggested.[7] These CEF parameters give rise to energy-level splittings from the GSs of 9.8 and 27.3 meV, which are incompatible with our INS measurements. We were unable to find a CEF scheme with this GS configuration that fitted both the INS and the magnetic susceptibility data.

We may now compare our results with those obtained from isostructural CeTX_3 compounds. Like $CeCoGe_3$, the CEF model for $CeRhGe_3$ predicts a GS which is an admixture of $|\pm\frac{5}{2}\rangle$ and $|\mp\frac{3}{2}\rangle$.[30] Both compounds have a significant B_4^4, 0.463 meV for $CeCoGe_3$ and 0.294 meV for $CeRhGe_3$, which leads to this mixing. In $CeRhGe_3$, the $|\pm\frac{3}{2}\rangle$ states are the largest components in the GS, whereas, for $CeCoGe_3$, it is $|\pm\frac{5}{2}\rangle$. In both compounds, the moments in the magnetically ordered state align along the c axis. However, B_2^0 is positive for $CeRhGe_3$, and a consideration of E_a predicts a moment lying in the ab plane. The alignment of the moment along c is ascribed to two-ion anisotropic exchange interactions. Unlike $CeCoGe_3$, the easy axis of the magnetic susceptibility is in the ab plane, despite the moment alignment along c below $T_{\rm N}$. The calculated value of $\langle\mu_z\rangle$ closely agrees with the result obtained from the magnetic neutron-diffraction measurements, and there is no evidence of a reduction in the cerium moment due to hybridization. In contrast to this, the CEF model for $CeCoGe_3$ correctly predicts the alignment of the ordered moment and the easy axis of the magnetic susceptibility. However, the observed moment is significantly reduced

compared to the calculated value of $\langle \mu_z \rangle$. The reduction in moment is not as drastic as in the other pressure-induced NCSs $CeRhSi_3$ and $CeIrSi_3$. For example, a CEF model of $CeRhSi_3$ (Ref. 37) predicts a moment of $0.92\mu_B$/Ce in the *ab* plane, whereas, a moment of $0.12\mu_B$/Ce in that direction is actually observed through neutron-diffraction studies.[38] This compound also has a very different magnetic structure, a spin-density wave with propagation vector $(0.215,0,\frac{1}{2})$. These results suggest that $CeCoGe_3$ has a degree of hybridization between that of $CeRhGe_3$ and $CeRhSi_3$. This is consistent with the fact that $CeRhSi_3$ is closer to a QCP, having an onset of superconductivity at 1.2 GPa,[9] whereas, $CeCoGe_3$ becomes superconducting at 5.5 GPa (Ref. 8) and $CeRhGe_3$ (Ref. 17) does not become superconducting up to 8.0 GPa. The linewidths of the CEF excitations give an indication of the hybridization strength between the conduction electrons and the excited states. The linewidths obtained for $CeCoGe_3$ at 25 K were 1.6(3) and 2.9(3) meV for transitions from the GS to ψ_2 and ψ_3, respectively. This is compared to values of 1.4(2) and 2.2(3) meV obtained for $CeRhGe_3$ (Ref. 30). The linewidth of the excitation to ψ_2 was similar in both compounds, whereas, the excitation to ψ_3 was broader in $CeCoGe_3$ than in $CeRhGe_3$. However, linewidths of 3.9(2) and 9.2(4) meV were obtained for the CEF excitations of $CeRhSi_3$ (Ref. 39), indicating stronger hybridization of all the states in the $J = \frac{5}{2}$ multiplet.

IV. CONCLUSIONS

We have studied the magnetic ordering in $CeCoGe_3$ using single-crystal neutron diffraction, inelastic neutron scattering, μSR, and magnetic susceptibility. The transition to magnetic ordering below T_{N1} is observed with the emergence of oscillations in zero-field μSR spectra. We fitted the temperature dependence of the internal magnetic fields to a model of a mean-field magnet. Single-crystal neutron-diffraction measurements reveal magnetic ordering with a propagation vector of $\mathbf{k} = (0,0,\frac{1}{2})$ below T_{N3}, $\mathbf{k} = (0,0,\frac{5}{8})$ for $T_{N3} < T < T_{N2}$, and $\mathbf{k} = (0,0,\frac{2}{3})$ for $T_{N2} < T < T_{N1}$. From a refinement of the integrated intensities, we suggest a two-up two-down magnetic structure below T_{N3} with moments of $0.405(5)\mu_B$/Ce along the *c* axis. Measurements of the (110) reflection indicate a ferromagnetic component between T_{N3} and T_{N1}. From this, we suggest a two-up one-down structure for the phase between T_{N2} and T_{N1}. INS measurements of polycrystalline $CeCoGe_3$ at low temperatures indicate two CEF excitations at 19 and 27 meV. At 4 K, we observe an additional peak at 4.5 meV due to spin-wave excitations. Above T_{N1}, this peak is not present, but quasielastic scattering is observed. A linear fit to the temperature dependence of the quasielastic linewidth gives an estimate of $T_K = 11(3)$ K. From an analysis of INS and magnetic-susceptibility data with a CEF model, we propose a CEF scheme for $CeCoGe_3$. We are also able to account for the spin-wave peak at 4.5 meV by the addition of an internal field along the *c* axis. The CEF scheme correctly predicts the direction of the ordered moment, but the observed magnetic moment at 2 K of $0.405(5)\mu_B$/Ce is reduced compared to the predicted moment of $1.01\mu_B$/Ce. We believe that the reduced moment is due to hybridization between the localized Ce^{3+} f electrons and the conduction band. From considering the moment reduction, we deduce that $CeCoGe_3$ has a hybridization strength between that of the localized antiferromagnet $CeRhGe_3$ and the NCS $CeRhSi_3$. $CeRhSi_3$ exhibits SC at lower applied pressure than $CeCoGe_3$, whereas, $CeRhSi_3$ does not exhibit SC up to at least 8.0 GPa. This is evidence for the important role of hybridization in the unconventional superconductivity of the $CeTX_3$ series.

ACKNOWLEDGMENTS

We acknowledge the EPSRC, U.K. for providing funding (Grant No. EP/I007210/1). D.T.A. and A.D.H. thank CMPC-STFC (Grant No. CMPC-09108) for financial support. We thank T. E. Orton for technical support, S. York for compositional analysis, and P. Manuel, B. D. Rainford, and K. A. McEwen for interesting discussions. Some of the equipment used in this research at the University of Warwick was obtained through the Science City Advanced Materials: Creating and Characterising Next Generation Advanced Materials Project, with support from Advantage West Midlands (AWM) and partly funded by the European Regional Development Fund (ERDF).

*m.smidman@warwick.ac.uk
†devashibhai.adroja@stfc.ac.uk
‡g.balakrishnan@warwick.ac.uk

[1] N. D. Mathur, F. M. Grosche, S. R. Julian, I. R. Walker, D. Freye, R. K. W. Haselwimmer, and G. G. Lonzarich, Nature (London) **394**, 39 (1998).
[2] C. Pfleiderer, Rev. Mod. Phys. **81**, 1551 (2009).
[3] E. Bauer, G. Hilscher, H. Michor, C. Paul, E. W. Scheidt, A. Gribanov, Y. Seropegin, H. Noël, M. Sigrist, and P. Rogl, Phys. Rev. Lett. **92**, 027003 (2004).
[4] L. P. Gor'kov and E. I. Rashba, Phys. Rev. Lett. **87**, 037004 (2001).
[5] E. Bauer and M. Sigrist, *Non-Centrosymmetric Superconductors: Introduction and Overview*, Lecture Notes in Physics (Springer-Verlag, Berlin, Heidelberg, 2012).
[6] V. K. Pecharsky, O.-B. Hyun, and K. A. Gschneidner, Phys. Rev. B **47**, 11839 (1993).
[7] A. Thamizhavel, T. Takeuchi, T. D. Matsuda, Y. Haga, K. Sugiyama, R. Settai, and Y. Ōnuki, J. Phys. Soc. Jpn. **74**, 1858 (2005).
[8] R. Settai, I. Sugitani, Y. Okuda, A. Thamizhavel, M. Nakashima, Y. Ōnuki, and H. Harima, J. Magn. Magn. Mater. **310**, 844 (2007).
[9] N. Kimura, K. Ito, K. Saitoh, Y. Umeda, H. Aoki, and T. Terashima, Phys. Rev. Lett. **95**, 247004 (2005).
[10] I. Sugitani, Y. Okuda, H. Shishido, T. Yamada, A. Thamizhavel, E. Yamamoto, T. D. Matsuda, Y. Haga, T. Takeuchi, R. Settai, and Y. Ōnuki, J. Phys. Soc. Jpn. **75**, 043703 (2006).
[11] F. Honda, I. Bonalde, S. Yoshiuchi, Y. Hirose, T. Nakamura, K. Shimizu, R. Settai, and Y. Ōnuki, Physica C **470**(Suppl. 1), S543 (2010).

[12]M.-A. Masson, H. Muranaka, T. Matsuda, T. Kawai, Y. Haga, G. Knebel, D. Aoki, G. Lapertot, F. Honda, R. Settai, J.-P. Brison, J. Flouquet, K. Shimizu, and Y. Onuki, Physica C **470**(Suppl. 1), S536 (2010).
[13]D. Eom, M. Ishikawa, J. Kitagawa, and N. Takeda, J. Phys. Soc. Jpn. **67**, 2495 (1998).
[14]T. Shimoda, Y. Okuda, Y. Takeda, Y. Ida, Y. Miyauchi, T. Kawai, T. Fujie, I. Sugitani, A. Thamizhavel, T. Matsuda, Y. Haga, T. Takeuchi, M. Nakashima, R. Settai, and Y. Ōnuki, J. Magn. Magn. Mater. **310**, 308 (2007).
[15]S. Doniach, Physica B & C **91**, 231 (1977).
[16]R. Settai, T. Takeuchi, and Y. Ōnuki, J. Phys. Soc. Jpn. **76**, 051003 (2007).
[17]T. Kawai, H. Muranaka, M.-A. Measson, T. Shimoda, Y. Doi, T. D. Matsuda, Y. Haga, G. Knebel, G. Lapertot, D. Aoki, J. Flouquet, T. Takeuchi, R. Settai, and Y. Ōnuki, J. Phys. Soc. Jpn. **77**, 064716 (2008).
[18]A. Thamizhavel, H. Shishido, Y. Okuda, H. Harima, T. D. Matsuda, Y. Haga, R. Settai, and Y. Ōnuki, J. Phys. Soc. Jpn. **75**, 044711 (2006).
[19]V. V. Krishnamurthy, K. Nagamine, I. Watanabe, K. Nishiyama, S. Ohira, M. Ishikawa, D. H. Eom, T. Ishikawa, and T. M. Briere, Phys. Rev. Lett. **88**, 046402 (2002).
[20]G. Knebel, D. Aoki, G. Lapertot, B. Salce, J. Flouquet, T. Kawai, H. Muranaka, R. Settai, and Y. Ōnuki, J. Phys. Soc. Jpn. **78**, 074714 (2009).
[21]M. Mizoo, T. Nishioka, H. Kato, and M. Matsumura, J. Phys.: Conf. Ser. **273**, 012009 (2011).
[22]K. Kaneko, N. Metoki, T. Takeuchi, T. D. Matsuda, Y. Haga, A. Thamizhavel, R. Settai, and Y. Ōnuki, J. Phys.: Conf. Ser. **150**, 042082 (2009).
[23]A. Das, R. K. Kremer, R. Pöttgen, and B. Ouladdiaf, Physica B **378–380**, 837 (2006).
[24]A. Yaouanc and M. Dalmas de Rèotier, *Muon Spin Rotation, Relaxation and Resonance*, International Series of Monographs on Physics Vol. 147 (Oxford University Press, Oxford, 2011).
[25]A. Coelho, *TOPAS-Academic* (Coelho Software, Brisbane, 2007).
[26]S. Blundell, *Magnetism in Condensed Matter*, Oxford Master Series in Condensed Matter (Oxford University Press, Oxford, 2001).
[27]F. L. Pratt, J. Phys.: Condens. Matter **19**, 456207 (2007).
[28]A. Wills, Physica B **276–278**, 680 (2000).
[29]J. Rodríguez-Carvajal, Physica B **192**, 55 (1993).
[30]A. D. Hillier, D. T. Adroja, P. Manuel, V. K. Anand, J. W. Taylor, K. A. McEwen, B. D. Rainford, and M. M. Koza, Phys. Rev. B **85**, 134405 (2012).
[31]K. W. Becker, P. Fulde, and J. Keller, Z. Phys. B **28**, 9 (1977).
[32]A. Krimmel, A. Severing, A. Murani, A. Grauel, and S. Horn, Physica B **180–181**, 191 (1992).
[33]K. W. H. Stevens, Proc. Phys. Soc. London, Sec. A **65**, 209 (1952).
[34]M. Hutchings, in *Solid State Physics: Advances in Research and Applications*, edited by F. Seitz and D. Turnbull (Academic, New York, 1964), Vol. 16, pp. 227–273.
[35]J. Jensen and A. Mackintosh, *Rare Earth Magnetism: Structures and Excitations*, International Series of Monographs on Physics (Clarendon, Oxford, 1991).
[36]G. Marusi, N. V. Mushnikov, L. Pareti, M. Solzi, and A. E. Ermakov, J. Phys.: Condens. Matter **2**, 7317 (1990).
[37]Y. Muro, M. Ishikawa, K. Hirota, Z. Hiroi, N. Takeda, N. Kimura, and H. Aoki, J. Phys. Soc. Jpn. **76**, 033706 (2007).
[38]N. Aso, H. Miyano, H. Yoshizawa, N. Kimura, T. Komatsubara, and H. Aoki, J. Magn. Magn. Mater. **310**, 602 (2007).
[39]D. T. Adroja, A. D. Hillier, V. K. Anand, E. A. Goremychkin, K. A. McEwen, B. D. Rainford, V. V. Krishnamurthy, and G. Balakrishnan, ISIS Facility Experimental Report No. RB820238, 2009 (unpublished).